The Role of Nd in Corrosion Properties of Mg-12Gd-2Zn-0.4Zr Alloys

Lixin Hong, Rongxiang Wang, and Xiaobo Zhang

To reveal the effect of Nd addition on corrosion properties of Mg-Gd-Zn-Zr alloys, the corrosion behavior of the as-cast Mg-12Gd-2Zn-xNd-0.4Zr ($x = 0$, 0.5, and 1 wt.%) alloys was investigated by using immersion and electrochemical measurements. The results show that the addition of Nd apparently refines and homogenizes the microstructure of the alloys. The corrosion resistance of the three alloys is improved in the initial 24 h corrosion process with increasing Nd addition according to hydrogen evolution results, later followed by an acceleration of corrosion with prolonging immersion time. During the 60 h immersion tests, the alloy without the addition of Nd exhibits the best corrosion resistance and the alloy with 0.5 wt.% Nd shows the highest corrosion rate, which are consistent with the electrochemical test results. The refined microstructure and increased fraction of the eutectic phase compromise the corrosion resistance of the alloys with Nd addition.

1. Introduction

Magnesium alloys have an extensive application prospect in automobile, rail transit, aerospace, and other fields by virtue of the advantages of low density, high specific strength, and good casting performance, as well as excellent machinability and weldability (Ref 1-3). However, magnesium is an extremely active metal with low standard electrode potential. Therefore, it has a high chemical reaction activity, suffering serious chemical corrosion in humid air and oceanic atmosphere (Ref 4). The poor corrosion resistance of magnesium alloys seriously hinders their further applications. In view of this, more attention is paid to the improvement of corrosion resistance.

Rare earth (RE) alloying is an effective way to improve the corrosion resistance of Mg alloys mainly due to the following effects: electrode potential, grain size, second phase, and corrosion product film (Ref 5-11). Compared with common alloying elements added in Mg alloys, the electrode potentials of RE elements (Gd: -2.40 V, Nd: -2.44 V) are close to that of Mg (-2.37 V), and their compounds have low electrode potentials, so as to help reducing galvanic corrosion (Ref 5, 6). After RE element was added to Mg alloys, the segregated RE element is located at the solid–liquid interface where the grain boundary grows, thus inhibiting the grain growth. So the addition of RE elements can reduce pitting and corrosion rate (Ref 7-9). Furthermore, the RE elements gathered at the grain boundary may form the second phase and affect the volume fraction and distribution of the second phase. When the volume fraction of the second phase is large, second phase with continuous network may act as corrosion barrier during corrosion process (Ref 10). In addition, adding RE elements can promote the formation of denser corrosion product films on the surface of Mg alloys, so as to further protect Mg alloys from corrosion effectively (Ref 11).

Moreover, long period stacking ordered (LPSO) structure and stacking faults (SFs) found in RE-containing Mg alloys in recent years have a significant impact on the corrosion properties of Mg alloys (Ref 12-17). In some Mg-Y-Zn alloys, the LPSO structure and Mg matrix with different potential form a micro-galvanic couple which accelerates corrosion of the alloys (Ref 18, 19). In some Mg-Gd-Zn alloys, the LPSO structure can regulate the corrosion behavior of Mg alloys (Ref 20-22). The higher the volume fraction of LPSO is, the lower the corrosion rate of the alloy and the more uniform the corrosion mode will be (Ref 23). The SFs structure in Mg-3Gd-1Zn-0.4Zr can also reduce corrosion rate (Ref 14).

A few studies have shown that adding a small amount of Nd into Mg alloys can optimize microstructure and enhance mechanical and corrosion properties (Ref 24, 25). In our previous study, the mechanical properties of Mg-12Gd-2Zn-xNd-0.4Zr ($x = 0$, 0.5, and 1 wt.%) were improved and the tension-compression yield asymmetry in reverse was significantly reduced by minor addition of Nd. In the present work, the corrosion properties were studied to reveal the role of Nd addition in corrosion behavior of the alloy.

2. Materials and Methods

Three groups of Mg-12Gd-2Zn-xNd-0.4Zr alloys (x=0, 0.5, 1 wt.%, denoted as Alloy 1, Alloy 2, and Alloy 3, respectively) were prepared by gravity casting method in an electric resistance furnace (MXD-10M). The raw materials were highly pure Mg, pure Zn, Mg-30 wt.% Gd, Mg-30 wt.% Zr, and Mg-30 wt.% Nd. Before smelting, the raw materials were dried in

Lixin Hong, Rongxiang Wang, and **Xiaobo Zhang**, School of Materials Science and Engineering, Nanjing Institute of Technology, Nanjing 211167, China; and Jiangsu Key Laboratory of Advanced Structural Materials and Application Technology, Nanjing 211167, China. Contact e-mails: xbxbzhang2003@163.com and xbzhang@njit.edu.cn.

an oven at 150 °C, and then pure Mg ingots were placed in a resistance crucible furnace. When the temperature reached 300 °C, a mixed gas of CO_2 and SF_6 was injected as the protective atmosphere. After the high-purity Mg ingots were completely melted, the Mg-Gd, Mg-Zr, and pure Zn were added into the molten metal subsequently, as well as Mg-Nd for Alloy 2 and Alloy 3. The molten metals were stirred for 5 min to make them homogeneous. After standing for 15-20 min, they were cast into the preheated metal mold. Finally, the ingots were taken out and cooled by water. The samples for microstructure observation and corrosion property characterization were cut by a wire cutting machine from the as-cast ingots.

The microstructures of the as-cast alloys were observed using optical microscope (OM, OLYMPUS GX51), scanning electron microscope (SEM, JSM-6360LV) equipped with energy-dispersive spectrometer (EDS, GENESIS 2000XM60). The volume fraction of eutectic phase and grain size was measured by using Image-Pro-Plus 6.0 software. The phases were analyzed by x-ray diffraction (XRD, Rigaku Ultima-IV) with Cu target. The operating voltage was 40 kV, the scanning angle ranged from 20 ° to 80 °, and the scanning speed was 6°/min.

Three parallel samples with dimension of $\Phi 14$ mm $\times$ 4 mm were polished and immersed in 3.5% NaCl solution at ambient temperature. The total immersion time was 60 h. The hydrogen evolution volume was recorded at intervals of 0.5 h for the first 2 h, at intervals of 2 h from 2 to 12 h, and then at intervals of 12 h for the subsequent immersion. The NaCl solution was renewed per 12 h to reduce the impact of increased pH value. The corrosion rates were calculated according to the following formula (Ref 26):

$$V_{\mathrm{corr}} = 95.05 \times \frac{V_H}{\rho \mathrm{AT}}$$

V_{corr} is the corrosion rate (mm/year); V_{H} is the amount of hydrogen evolution (mL); ρ is the density of the alloy (g/cm^3); A is the total surface area of the soaking sample (cm^2); T is the immersion time (h).

The corrosion specimens were cleaned in boiling chromic acid solution (200 g/L CrO_3 + 10 g/L $AgNO_3$) for 5 min to remove the corrosion products. The corrosion morphologies were observed from corroded surface and cross section by SEM, and the corrosion product elements were analyzed by EDS.

The corrosion properties of the Mg-12Gd-2Zn-xNd-0.4Zr alloys were also characterized in 3.5% NaCl solution by electrochemical tests using an electrochemical workstation (Ametek PARSTAT 2273). The EIS tests were carried out from 100 MHz to 10 kHz at the open-circuit potential. Then, the potentiodynamic polarization curves were measured in a standard three-electrode configuration, using the specimen as a working electrode with 1 cm^2 exposed surface. The platinum flake was used as counter electrode, and the saturated calomel electrode was used as a reference electrode. Polarization tests at ambient temperature were carried out with a scanning rate of 0.5 mV/s after the samples were immersed for 30 min.

3. Results

3.1 Microstructures

Figure 1 shows the OM and SEM images of the as-cast Mg-12Gd-2Zn-xNd-0.4Zr alloys. The alloys are mainly composed of α-Mg matrix, eutectic phase at the grain boundaries, and lamellar structures mostly distributed at the outer edge of the matrix grains which can be clearly observed in the SEM images embedded in Fig. 1(b), (d), and (f). According to the results of transmission electron microscope observation, the lamellar structures have been identified as SFs which were reported elsewhere (Ref 27). The eutectic phase distributed at grain boundaries shows discontinuous mesh morphology. It is composed of α-Mg and β phases in alternating distribution, presenting a fishbone shape. The volume fractions of eutectic phases of Alloy 1, 2, and 3 are 5.7%, 11.1%, and 14.3%, respectively, indicating that Nd addition increases the volume fraction of the eutectic phase.

Table 1 lists the compositions of the marked areas (α-Mg matrix, eutectic phase, and SFs) in Fig. 1 analyzed by EDS. The contents of Gd and Zn in the alloys from high to low are as follows: the eutectic phase > the SFs > the matrix. With the addition of Nd, the content of Gd in SFs increases obviously, and the content of Zn increases slightly. More Nd is found in the eutectic phase as compared to the matrix and SFs. The grain size distribution of the alloys is shown in Fig. 2. The grain sizes of Alloy 1, 2 and 3 range from 21 to 90 μm, from 11 to 50 μm, and from 11 to 40 μm, respectively, which shows the important role of element Nd in refining and homogenizing microstructure. The average grain size of the alloy with 0% Nd is 56.6 μm, and it reduces to 29.0 μm and 25.8 μm with 0.5% and 1% Nd addition, respectively, showing obvious grain refinement effect caused by Nd.

3.2 Corrosion Properties

The polarization curves of the alloys tested in 3.5% NaCl solution are shown in Fig. 3, and the potential and current density fitted by Tafel extrapolation are also presented. The corrosion potential of the alloys reduces with increasing Nd addition, which means lower corrosion resistance in terms of corrosion thermodynamics. However, according to corrosion kinetics, a lower current density means a better corrosion resistance. The current density of Alloy 1 is the lowest compared with that of Alloy 2 and 3, indicating the best corrosion resistance, while the Alloy 2 with the highest current density shows the worst corrosion resistance. The results indicate that the corrosion resistance reduces with Nd addition, and that of the Alloy 3 with 1 wt.% Nd is better than that of the Alloy 2 with 0.5 wt.% Nd.

The Nyquist curves of Mg-12Gd-2Zn-xNd-0.4Zr alloys are presented in Fig. 4. The radius of high frequency capacitance is related to the corrosion resistance of Mg alloys. The larger the radius is, the better the corrosion resistance will be. The order of capacitance radius from large to small is as follows: Alloy 1 > Alloy 3 > Alloy 2. The capacitance radius of Alloy 1 is the largest, suggesting the best corrosion resistance. According to Nyquist curves, the corrosion resistance trend of the alloys is consistent with that of the polarization curves, and the order of corrosion resistance of the alloys from strong to weak is as follows: Alloy 1 > Alloy 3 > Alloy 2.

The equivalent circuit is shown in Fig. 5 to analyze the corrosion behavior of the alloys and the fitting data of the EIS spectra are shown in Table 2. The three resistance components R_s, R_{ct}, and R_f represent the solution resistance, charge transfer resistance, and film resistance, respectively. The higher the value of R_{ct} and R_f, the better the corrosion resistance of the alloy. The double-layer capacity (C_{dl}) value represents the area
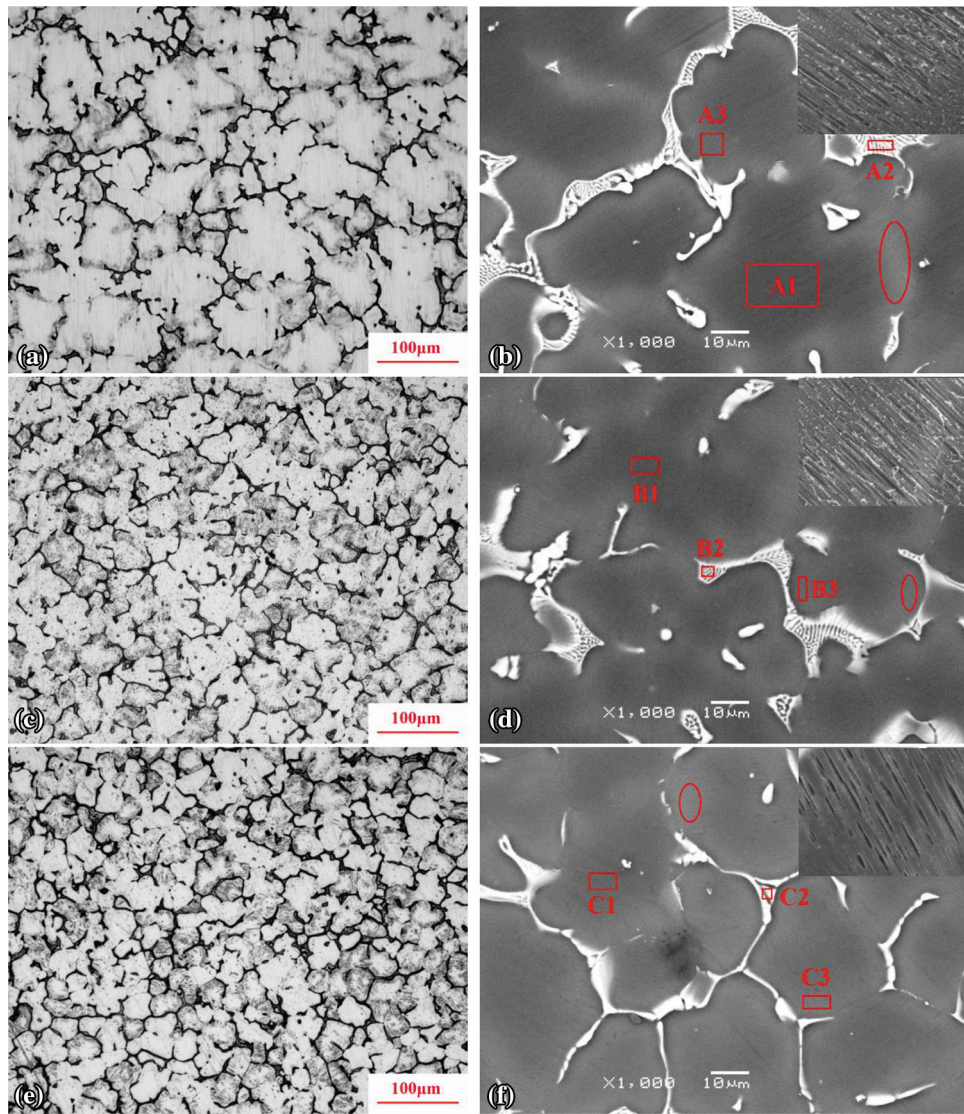
Fig. 1 OM (a, c, e) and SEM (b, d, f) images of the alloys (a, b) Alloy 1, (c, d) Alloy 2, (e, f) Alloy 3

Table 1 Chemical compositions (wt.%) of the various areas marked in Fig. 1

Alloys	Areas	Gd	Zn	Zr	Nd	Mg
Alloy 1	A1	4.03	1.07	1.94	0	Bal.
	A2	37.20	8.65	0.37	0	Bal.
	A3	8.04	1.47	0.92	0	Bal.
Alloy 2	B1	5.88	1.14	0.79	1.00	Bal.
	B2	38.59	9.47	0.81	3.26	Bal.
	B3	12.28	1.31	0.29	0.47	Bal.
Alloy 3	C1	5.05	1.05	1.97	0.83	Bal.
	C2	36.05	10.29	0.67	4.03	Bal.
	C3	16.13	2.81	0.14	2.19	Bal.

Fig. 2 The grain size distribution of the alloys

of corrosion reaction, and higher C_{dl} value means larger corrosion area on the surface of the alloy (Ref 26). The film capacity (C_f) value is relative to the thickness of film, and low C_f value means the film is more compact. As is shown in Table 2, the R_s values of the three alloys show little difference.
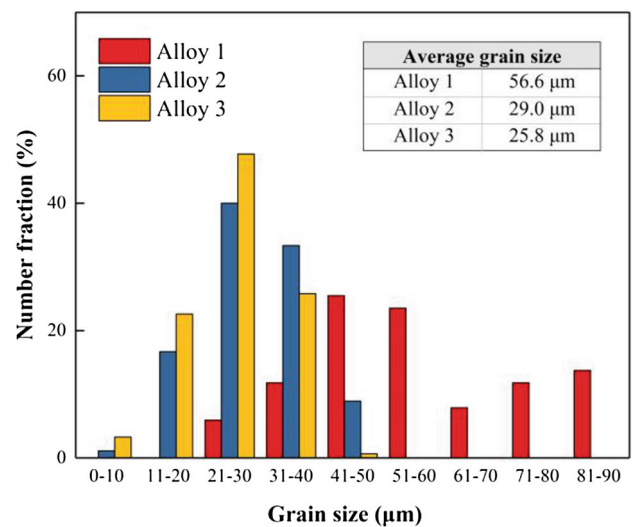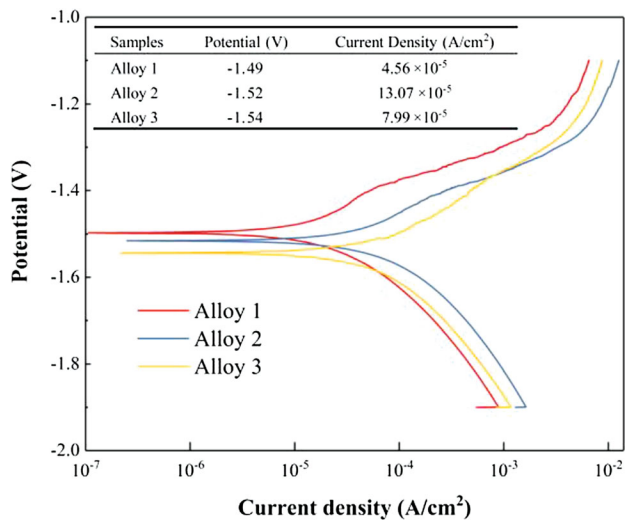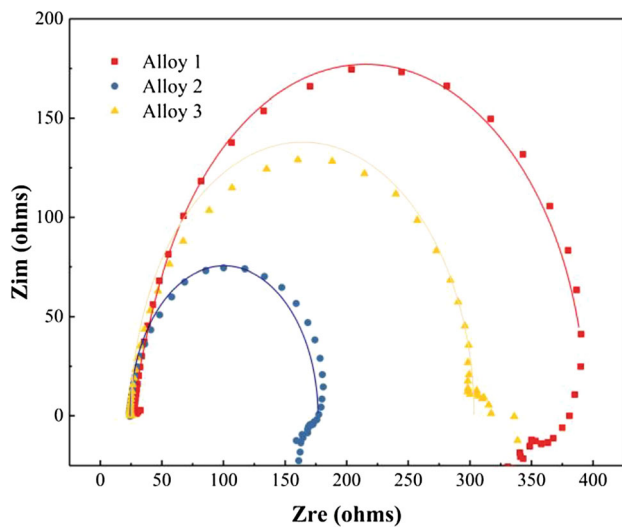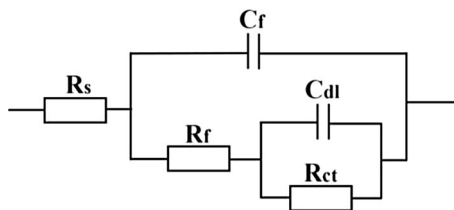
Samples	Potential (V)	Current Density (A/cm^2)
Alloy 1	-1.49	4.56×10^{-5}
Alloy 2	-1.52	13.07×10^{-5}
Alloy 3	-1.54	7.99×10^{-5}

Fig. 3 Polarization curves of the alloys tested in 3.5% NaCl solution

Fig. 4 Nyquist curves of the as-cast alloys immersed in 3.5% NaCl solution

Fig. 5 Equivalent circuit models of fitting EIS data for the as-cast alloys

The R_{ct} value of Alloy 1 is the highest, and the values of C_f and C_{dl} are the lowest which show that the corrosion resistance of Alloy 1 is the best. The R_f of Alloy 2 is the lowest, and that of Alloy 3 is the highest, which are not consistent with the corrosion resistance trend of alloys. R_f is an influencing factor of the corrosion resistance of alloys, but the corrosion properties of alloys cannot be determined by it. The C_{dl} of

the alloys increases after element Nd was added, indicating that the corrosion area on the surface increases.

Figure 6 shows the hydrogen evolution curves of the alloys. The hydrogen evolution curves are relatively gentle at the initial stage of corrosion process, in which the hydrogen evolution volume of Alloy 1 is the highest and always higher than that of Alloy 2 and Alloy 3 during the initial 24 h immersion. This indicates that the addition of Nd improved the corrosion resistance of the alloy at the initial stage of immersion experiment. With the increase in Nd content, the corrosion resistance of Alloy 3 (1% Nd) is slightly improved compared with that of Alloy 2 (0.5% Nd). After 24 h immersion, the hydrogen evolution volume of Alloy 2 and Alloy 3 increases faster and gradually exceeds that of Alloy 1. The hydrogen evolution volume from large to small for the 60 h immersion shows the following sequence: Alloy 2 > Alloy 3 > Alloy 1. According to the hydrogen evolution volume of 60 h, the corrosion rate calculated by the formula is shown in Fig. 7. The corrosion rates of Alloy 1, 2, 3 are 1.03, 1.37, and 1.27 mm/y, respectively.

Figure 8 shows the surface corrosion morphologies of the alloys after immersion test with and without corrosion products. Corrosion products are aggregated on the surface of the alloys. After removing corrosion products, pitting is visible for all the alloys, but no serious localized corrosion occurred, and the corroded surfaces are relatively uniform.

Figure 9 shows the cross section of the specimens after immersion test. The thickness of corrosion products film shows the following sequence: Alloy 2 > Alloy 3 > Alloy 1. It can be observed that the matrix grains were corroded preferentially. Eutectic phase plays a vital role in protecting the matrix grains: If the eutectic phase is continuously distributed at the grain boundary, the adjacent matrix grains will be corroded only when the eutectic phase dissolves.

4. Discussion

The microstructure becomes more uniform and the eutectic phase distributes more continuously at the grain boundaries with increasing Nd addition. This is mainly because that Nd gathers at the solid–liquid interface and inhibits grain growth of the Mg alloys, making the microstructure fine and uniform (Ref 28, 29).

Relevant studies have shown that Nd can effectively improve the corrosion resistance of Mg alloys (Ref 5, 24, 25). However, the Alloy 2 and Alloy 3 do not exhibit better corrosion resistance after element Nd was added in this study. Microstructure, including grain size and phase distribution, plays a vital role in the corrosion resistance of the alloy (Ref 30, 31). Alloy 1 has the largest grain size and uneven microstructure distribution, so it is easy to form the galvanic corrosion mechanism of large anode and small cathode (anode: the matrix grains, cathode: the eutectic phase) (Ref 32). After the addition of Nd in the alloy, the grain size of the alloy is smaller, and the microstructure becomes uniform, leading to more uniform corrosion, as well as reducing the pitting trend of the alloy. However, the overall corrosion resistance of the alloys with Nd addition is reduced even though they have finer microstructures, which is attributed to the increment of the eutectic phase (Ref 33). The distribution of eutectic phase has a great influence on the corrosion resistance of the alloy. Generally, eutectic

Table 2 Fitting results of EIS data

| Alloy	R_s , Ω cm^2	C_f , μF cm^{-2}	R_f , Ω cm^2	C_{dl} , μF cm^{-2}	R_{ct} , Ω cm^2
Alloy 1	28.4	8.0	110.6	4.2	228.3
Alloy 2	23.8	11.6	55.3	7.0	95.0
Alloy 3	24.6	10.9	153.4	13.4	128.5
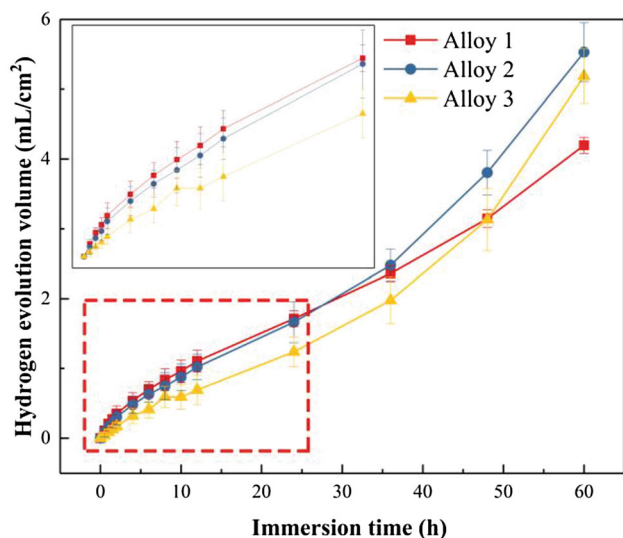
Fig. 6 Hydrogen evolution of the as-cast alloys immersed in 3.5% NaCl solution
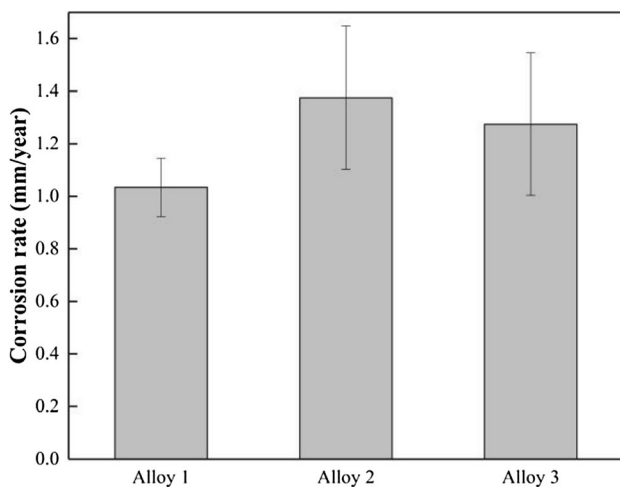
Fig. 7 Corrosion rate of the as-cast alloys after immersion in 3.5% NaCl solution for 60 h

phase acts a dual role in preventing the Mg alloy from dissolving and acting as cathode in the corrosion process of the alloy. If the volume fraction of eutectic phase is large and the eutectic phase is to some degree continuously distributed along the matrix grain boundaries, the eutectic phase can serve as a corrosion barrier and effectively reduce the corrosion rate. Otherwise, it will accelerate the corrosion of Mg alloy (Ref 34). In the present work, the volume fraction of eutectic phase increases with Nd addition, and its distribution is discontinuous for Alloy 2, which could not play a role in reducing the corrosion rate but intensified the galvanic corrosion of the alloy. Nevertheless, for Alloy 3, the continuity of the eutectic phase is better as compared to that of Alloy 2, as shown in Fig. 1, hence, showing better corrosion resistance than Alloy 2 due to more corrosion barrier shown in Fig. 9(c) and finer microstructure.

In the early stage of corrosion, Nd mostly exists in the second phase as a cathode, which reduces the galvanic corrosion to a certain extent. At this time, the passivation film is easily formed at the corrosion interface, which hinders the corrosion of the alloy, thus improves the corrosion resistance of the alloy. In the 2-24 h hydrogen evolution experiment, Alloy 3 has the lowest corrosion rate and the best corrosion resistance. In the later stage of the corrosion process, with the dissolution of the passivation film, the corrosion solution gradually penetrates into the uncorroded substrate, and a large number of galvanic couples formed due to more eutectic phase, which eventually results in the increase in the corrosion rate of Alloy 2 and Alloy 3.

The Nyquist curves of the three alloys show only one high-frequency capacitance loop, indicating that the corrosion mechanism of the three alloys is the same. The high-frequency capacitance loop corresponds to the charge transfer process during the corrosion process of the alloy (Ref 35). In 3.5% NaCl solution, the main corrosion mechanism of the alloy is galvanic corrosion: α-Mg matrix acts as the anode and eutectic phase acts as the cathode. The schematic view of the corrosion mechanism of the alloys is shown in Fig. 10. In the early stage of corrosion, the following reaction occurs at the interface between the sample and solution: (Ref 36, 37)

$$Mg + 2H_2O = Mg(OH)_2 + H_2 \uparrow$$
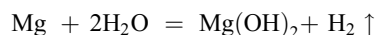
In Fig. 10(b), the α-Mg matrix in the surface corrodes first. Then, the generated $Mg(OH)_2$ is deposited on the corrosion surface, showing R_f in the equivalent circuit diagram, which can prevent corrosion and reduce the corrosion rate of the alloy. It can also be easily seen from the hydrogen evolution curve of the alloy during 2-24 h immersion that the volumes of hydrogen rise slightly and the corrosion rate is low. During 24-60 h immersion, the volumes of hydrogen gradually increase, which is ascribed to that as the immersion prolongs, the reaction occurs as follows:

$$Mg(OH)_2 + 2Cl^- = MgCl_2 + 2OH^-$$
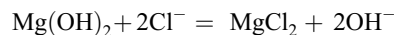
In the studies of Mg-Gd-Zn-Zr alloy, SFs can prevent the corrosion of the alloy and cause uniform corrosion on the surface (Ref 38, 39). SFs can act as a cathode to inhibit the corrosion of the alloy, so Mg alloys with SFs have better corrosion resistance than the alloys without SFs (Ref 14). $Mg(OH)_2$ gradually dissolves and generates new galvanic corrosion at the interface. When the SFs contact with the NaCl solution, they act as a cathode and the matrix around them corrodes preferentially, as shown in Fig. 10(c). In the present
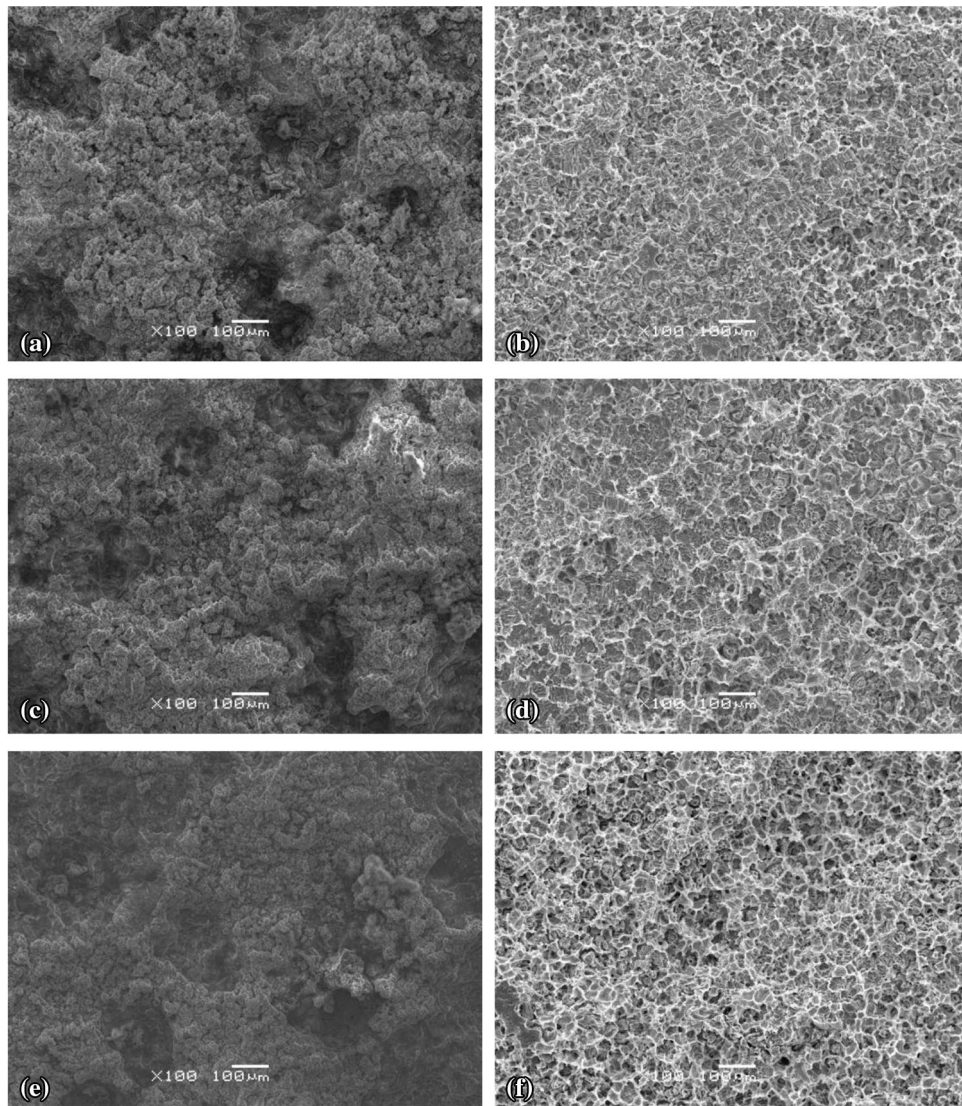
Fig. 8 Corrosion morphologies of the as-cast Mg alloys after immersion in 3.5% NaCl solution for 60 h. (a, b) Alloy 1, (c, d) Alloy 2, (e, f) Alloy 3 before (a, c, e) and after (b, d, f) removing corrosion products

work, all the three alloys have SFs which are probably beneficial for the corrosion resistance.

With prolonging immersion time, the two chemical reactions reach a reaction equilibrium. When the matrix exposed in NaCl solution is completely corroded, as well as the SFs, the eutectic phase begins to corrode or even peels off. Then, the matrix grains under the eutectic phase continue to corrode, as shown in Fig. 10(d). Therefore, the corrosion morphologies of the alloys are relatively uniform as presented in Fig. 8.

5. Conclusion

1. The as-cast Mg-12Gd-2Zn-xNd-0.4Zr alloys mainly consist of α-Mg matrix, eutectic phase, and stacking faults. After the addition of Nd, the microstructure is refined and homogenized, and the volume fraction of the eutectic phase increases.

2. After the addition of Nd, the corrosion resistance of the alloy increases at the initial stage of corrosion process, and passivation film is formed at the interface between the sample and the NaCl solution, which reduces the corrosion rate of the alloy. With the dissolution of the passivation film, the corrosion gradually penetrates into the substrate, and the corrosion rate of the alloy is higher than that of the alloy without Nd addition which is mainly due to more discontinuous eutectic phase.

3. During the 60 h immersion in 3.5% NaCl solution tests, the corrosion resistance of the alloys is in the following order: Alloy 1 > Alloy 3 > Alloy 2, which can be attributed to the comprehensive impacts of grain size, volume fraction, and distribution of eutectic phase caused by Nd addition.

4. The alloys present relatively uniform corrosion mode due to the stacking faults formed at the outer edge of matrix grains and eutectic phase distributed at matrix grain boundaries.
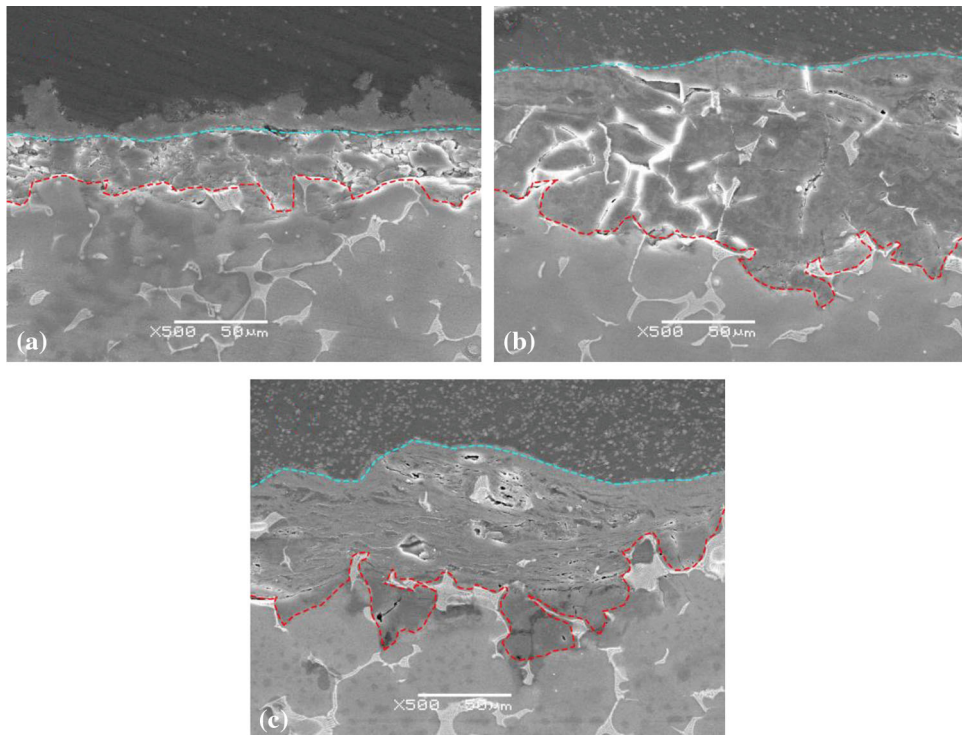
Fig. 9 Corrosion cross section of the as-cast Mg alloys after immersion in 3.5% NaCl solution for 60 h. (a) Alloy 1, (b) Alloy 2, (c) Alloy 3
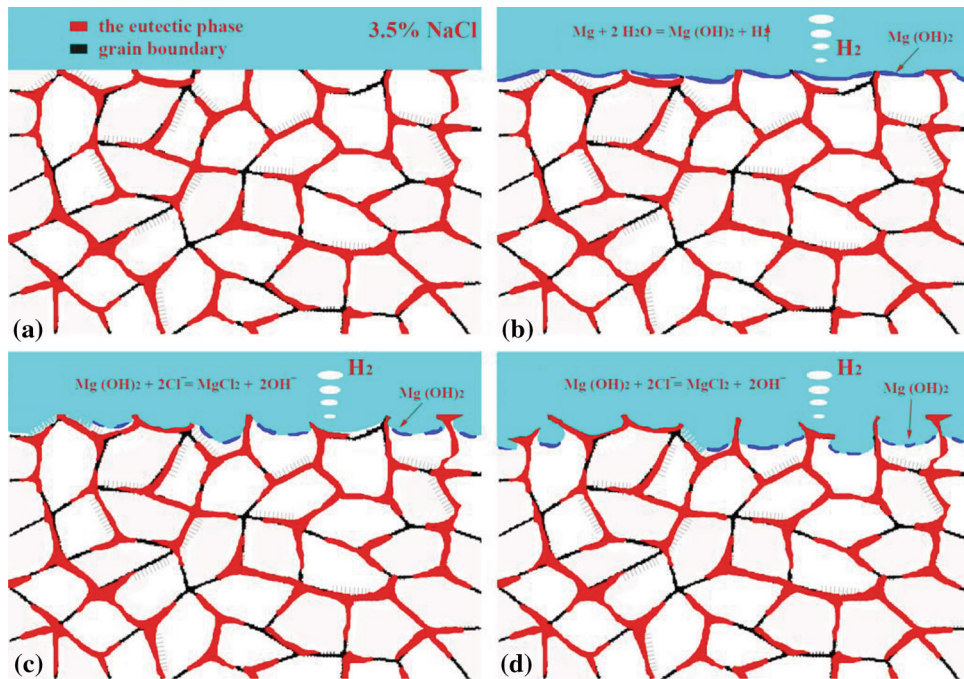
Fig. 10 Corrosion schematic of the as-cast Mg alloys

References

1. D.K. Xu, E.H. Han and Y.B. Xu, Effect of Long–Period Stacking Ordered Phase on Microstructure, Mechanical Property and Corrosion Resistance of Mg Alloys: A Review, *Prog. Nat. Sci-Mater.*, 2016, **26**(2), p 117–128. https://doi.org/10.1016/j.pnsc.2016.03.006
2. Z. Hu, Z. Yin, Z. Yin, B.B. Tang, X. Huang, H. Yan, H.G. Song, C. Luo and X.H. Chen, Influence of Sm Addition on Microstructural and Mechanical Properties of as-extruded Mg-9Li-5Al Alloy, *J. Alloy.*

Compds., 2020, **842**, p 155836. https://doi.org/10.1016/j.jallcom.2020.155836

3. D.X. Liu, D.L. Yang, X.L. Li and S.W. Hu, Mechanical Properties, Corrosion Resistance and Biocompatibilities of Degradable Mg–RE Alloys: A Review, *J. Mater. Res. Technol.*, 2019, **8**(1), p 1538–1549. https://doi.org/10.1016/j.jmrt.2018.08.003

4. Q.T. Jiang, D.Z. Lu, N. Wang, X.T. Wang, J. Zhang, J.Z. Duan and B.R. Hou, The Corrosion Behavior of Mg–Nd Binary Alloys in the Harsh Marine Environment, *J. Magnes. Alloy.*, 2020 https://doi.org/10.1016/j.jma.2019.12.010

5. J.S. Xie, J.H. Zhang, Z.H. You, S.J. Liu, K. Guan, R.Z. Wu, J. Wang and J. Feng, Towards Developing Mg Alloys with Simultaneously Improved Strength and Corrosion Resistance via RE Alloying, *J. Magnes. Alloy.*, 2020 https://doi.org/10.1016/j.jma.2020.08.016

6. S.Q. Yin, W.C. Duan, W.H. Liu, L. Wu, J.M. Yu, Z.L. Zhao, M. Liu, P. Wang, J.Z. Cui and Z.Q. Zhang, Influence of Specific Second Phases on Corrosion Behaviors of Mg–Gd–Zr alloys, *Corros. Sci.*, 2020, **166**, p 108419. https://doi.org/10.1016/j.corsci.2019.108419

7. J.F. Wang, Y. Li, S. Huang, Y.Y. Wei, X.F. Xi, K.Y. Cai and F.S. Pan, Effects of Y on the Microstructure, Mechanical and Bio–corrosion Properties of Mg–Zn–Ca Bulk Metallic Glass, *J. Mater. Sci. Technol.*, 2014, **30**(12), p 1255–1261. https://doi.org/10.1016/j.jmst.2014.11.007

8. L.Z. Liu, X.H. Chen, J.F. Wang, L.Y. Qiao, S.Y. Gao, K. Song, C.Y. Zhao, X.F. Liu, D. Zhao and F.S. Pan, Effects of Y and Zn Additions on Electrical Conductivity and Electromagnetic Shielding Effectiveness of Mg–Y–Zn Alloys, *J. Mater. Sci. Technol.*, 2019, **35**(6), p 1074–1080. https://doi.org/10.1016/j.jmst.2018.12.010

9. S.M. Ashrafizadeh, R. Mahmudi and A.R. Geranmayeh, A Comparative Study on the Effects of Gd, Y and La rare–earth Elements on the Microstructure and Creep Behavior of AZ81 Mg Alloy, *Mater. Sci. Eng. A*, 2020, **790**, p 139712. https://doi.org/10.1016/j.msea.2020.139712

10. J.Y. Zhang, B. Jiang, Q.S. Yang, D. Huang, A.T. Tang, F.S. Pan and Q.Y. Han, Role of second phases on the corrosion resistance of Mg–Nd–Zr alloys, *J. Alloy. Compd.*, 2020, **849**, p 156619. https://doi.org/10.1016/j.jallcom.2020.156619

11. W.J. Liu, F.H. Cao, L.R. Chang, Z. Zhang and J.Q. Zhang, Effect of Rare Earth Element Ce and La on Corrosion Behavior of AM60 Magnesium Alloy, *Corros. Sci.*, 2009, **51**(6), p 1334–1343. https://doi.org/10.1016/j.corsci.2009.03.018

12. Z.H. Han, K. Zhang, J. Yang, R. Wei, Y.X. Liu and C.J. Zhang, The Anodic Role of Ni–Containing LPSO Phases During the Microgalvanic Corrosion of $Mg_{98}Gd_{1.5}Ni_{0.5}$ Alloy, *J. Mater. Eng. Perform.*, 2019, **28**, p 2451–2458. https://doi.org/10.1007/s11665-019-04018-x

13. Y.J. Wang, Y. Zhang, P.P. Wang, D. Zhang, B.W. Yu, Z. Xu and H.T. Jiang, Effect of LPSO Phases and Aged–precipitations on Corrosion Behavior of as–forged Mg–6Gd–2Y–1Zn–0.3Zr Alloy, *J. Mater. Res. Technol.*, 2020, **9**(4), p 7087–7099. https://doi.org/10.1016/j.jmrt.2020.05.048

14. X.B. Zhang, J.W. Dai, R.F. Zhang, Z.X. Ba and B. Nick, Corrosion Behavior of Mg–3Gd–1Zn–0.4Zr Alloy with and Without Stacking Faults, *J. Magnes. Alloy.*, 2019, **7**(2), p 240–248

15. L. Zhao, W. Chen, J.W. Dai, Z.Z. Wang and X.B. Zhang, Effects of Heat Treatment on Corrosion and Wear Behaviors of Mg–6Gd–2Zn–0.4Zr Alloy in Simulated Body Fluid, *J. Mater. Eng. Perform.*, 2017, **26**, p 5501–5510. https://doi.org/10.1007/s11665-017-2975-1

16. X.B. Zhang, J.W. Dai, Q.S. Dong, Z.X. Ba and Y.J. Wu, Corrosion Behavior and Mechanical Degradation of As-extruded Mg-Gd-Zn-Zr Alloys for Orthopedic Application, *J. Biomed. Mater. Res. B*, 2020, **1088**, p 698–708. https://doi.org/10.1002/jbm.b.34424

17. X.B. Zhang, Z.X. Ba, Q. Wang, Y.J. Wu, Z.Z. Zhang and Q. Wang, Uniform Corrosion Behavior of GZ51K Alloy with Long Period Stacking Ordered Structure for Biomedical Application, *Corros. Sci.*, 2014, **88**, p 1–5. https://doi.org/10.1016/j.corsci.2014.07.004

18. L.S. Wang, J.H. Jiang, H. Liu, B. Saleh and A.B. Ma, Microstructure Characterization and Corrosion Behavior of Mg–Y–Zn Alloys With Different Long Period Stacking Ordered Structures, *J. Magnes. Alloy.*, 2020, **8**(4), p 1208–1220. https://doi.org/10.1016/j.jma.2019.12.009

19. J.S. Zhang, J.D. Xu, W.L. Cheng, C.J. Chen and J.J. Kang, Corrosion Behavior of Mg–Zn–Y Alloy with Long–period Stacking Ordered Structures, *J. Mater. Sci. Technol.*, 2012, **28**(12), p 1157–1162. https://doi.org/10.1016/S1005-0302(12)60186-8

20. J. Liu, L.X. Yang, C.Y. Zhang, B. Zhang, T. Zhang, Y. Li, K.M. Wu and F.H. Wang, Role of the LPSO Structure in the Improvement of Corrosion Resistance of Mg–Gd–Zn–Zr Alloys, *J. Alloy. Compd.*, 2019, **782**(25), p 648–658. https://doi.org/10.1016/j.jallcom.2018.12.233

21. X.B. Zhang, Z.X. Ba, Z.Z. Wang and Y.J. Xue, Microstructures and Corrosion Behavior of Biodegradable Mg–6Gd–xZn–0.4Zr Alloys with and Without long Period Stacking Ordered Structure, *Corros. Sci.*, 2016, **105**, p 68–77. https://doi.org/10.1016/j.corsci.2016.01.004

22. J.F. Wang, W.Y. Jiang, Y. Ma, Y. Li and S. Huang, Substantial Corrosion Resistance Improvement in heat–Treated Mg–Gd–Zn Alloys with a long Period Stacking Ordered Structure, *Mater. Chem. Phys.*, 2018, **203**, p 352–361. https://doi.org/10.1016/j.matchemphys.2017.09.035

23. X.B. Zhang, Q. Wang, F.B. Chen, Y.J. Wu, Z.Z. Wang and Q. Wang, Relation Between LPSO Structure and Biocorrosion Behavior of Biodegradable GZ51K Alloy, *Mater. Lett.*, 2015, **138**, p 212–215. https://doi.org/10.1016/j.matlet.2014.09.133

24. Z. Yin, R.H. He, Y. Chen, Z. Yin, K. Yan, K. Wang, H. Yan, H.G. Song, C.X. Yin, H.Y. Guan, C. Luo and Z.H.U.C. Luc, Effect of Surface Micro-Galvanic Corrosion and Corrosive Film on the Corrosion Resistance of AZ91-xNd Alloys, *Appl. Surf. Sci.*, 2021, **536**, p 147761. https://doi.org/10.1016/j.apsusc.2020.147761

25. P. Dinesh, S. Manivannan, S.P. Kumaresh Babu and S. Natarajan, Effect of Nd on the Microstructure and Corrosion Behaviour of Mg-9Li-3Al Magnesium alloy in 3.5 wt.% NaCl Solution, *Mater. Today Proc.*, 2019, **15**(1), p 126–131. https://doi.org/10.1016/j.matpr.2019.05.034

26. Y.F. Luo, Y.L. Deng, L.Q. Guan, L.Y. Ye and X.B. Guo, The Microstructure and Corrosion Resistance of as–extruded Mg–6Gd–2Y–(0–1.5) Nd–0.2Zr Alloys, *Mater. Des.*, 2020, **186**(15), p 108289. https://doi.org/10.1016/j.matdes.2019.108289

27. L.X. Hong, R.X. Wang and X.B. Zhang, Effects of Nd on Microstructure and Mechanical Properties of as-cast Mg-12Gd-2Zn-xNd-0.4Zr Alloys with Stacking Faults, *J. Miner. Metall. Mater Int*, 2021 https://doi.org/10.1007/s12613-021-2264-8

28. J. Wei, Q.D. Wang, L. Zhang, D.D. Yin, B. Ye, H.Y. Jiang and W.J. Ding, Microstructure Refinement of Mg–Al–RE alloy by Gd Addition, *Mater. Lett.*, 2019, **246**, p 125–128. https://doi.org/10.1016/j.matlet.2019.02.126

29. X.Y. Hu, P.H. Fu, S. David, L.M. Peng, M. Sun and M.X. Zhang, On Grain Coarsening and Refining of the Mg–3Al alloy by Sm, *J. Alloy. Compd.*, 2016, **663**, p 387–394. https://doi.org/10.1016/j.jallcom.2015.11.193

30. Z. Zhu, J.F. Zhu, Y.J. Nie, X. Li, J.L. Cheng and X.B. Zhang, Effects of Annealing on Mechanical and Corrosion Properties of as-extruded NQZ310K Alloy, *J. Mater. Eng. Perform.*, 2020, **29**, p 925–932. https://doi.org/10.1007/s11665-020-04643-x

31. Z. Hu, R.L. Liu, S.K. Kairy, X. Li, H. Yan and N. Birbilis, Effect of Sm Additions on the Microstructure and Corrosion Behavior of Magnesium Alloy AZ91, *Corros. Sci.*, 2019, **149**, p 144–152. https://doi.org/10.1016/j.corsci.2019.01.024

32. G.L. Song, B. Johannesson, S. Hapugoda and D. StJohn, Galvanic Corrosion of Magnesium alloy AZ91D in Contact with an Aluminium Alloy, Steel and Zinc, *Corros. Sci.*, 2004, **46**(4), p 955–977. https://doi.org/10.1016/S0010-938X(03)00190-2

33. H. Feng, S.H. Liu, Y. Du, T. Lei, R.C. Zeng and T.C. Yuan, Effect of the Second Phases on Corrosion Behavior of the Mg–Al–Zn Alloys, *J. Alloys Compd.*, 2017, **695**, p 2330–2338. https://doi.org/10.1016/j.jallcom.2016.11.100

34. D.B. Liu, Y.C. Liu, Y. Huang, R. Song and M.F. Chen, Effects of Solidification Cooling rate on the Corrosion Resistance of Mg–Zn–Ca Alloy, *Prog. Nat. Sci-Mater.*, 2014, **24**(5), p 452–457. https://doi.org/10.1016/j.pnsc.2014.08.002

35. H. Zengin and Y. Turen, Effect of Y Addition on Microstructure and Corrosion Behavior of Extruded Mg–Zn–Nd–Zr alloy, *J. Magnes. Alloy.*, 2020, **8**(3), p 640–653. https://doi.org/10.1016/j.jma.2020.06.004

36. G. Song, Recent Progress in Corrosion and Protection of Magnesium Alloys, *Adv. Eng. Mater.*, 2005, **7**(7), p 563–586. https://doi.org/10.1002/adem.200500013

37. L.T. Yu, Z.H. Zhao, C.K. Tang, W. Li, C. You and M.F. Chen, The Mechanical and Corrosion Resistance of Mg–Zn–Ca–Ag Alloys: The Influence of Ag Content, *J. Mater. Res. Technol.*, 2020, **9**(5), p 10863–10875. https://doi.org/10.1016/j.jmrt.2020.07.088

38. L. Zhang, J.H. Zhang, C. Xu, Y.B. Jing, J.P. Zhuang, R.Z. Wu and M.L. Zhang, Formation of Stacking Faults for Improving the Performance of Biodegradable Mg–Ho–Zn Alloy, *Mater. Lett.*, 2014, **133**, p 158–162. https://doi.org/10.1016/j.matlet.2014.06.171

39. X.B. Zhang, S. Kairy, J.W. Dai and N. Birbilis, A Closer Look at the Role of Nanometer Scale Solute-Rich Stacking Faults in the Localized Corrosion of a Magnesium Alloy GZ31K, *J. Electrochem Soc.*, 2018, **165**(7), p 310–316. https://doi.org/10.1149/2.0391807jes